Biomaterials Science

ROYAL SOCIETY OF CHEMISTRY

PAPER

View Article Online
View Journal | View Issue

Cite this: *Biomater. Sci.*, 2022, **10**, 5504

Rhoifolin loaded in PLGA nanoparticles alleviates oxidative stress and inflammation *in vitro* and *in vivo*†

Eveen Al-Shalabi, Samah Abusulieh, Alaa M. Hammad and Suhair Sunoqrot *

Rhoifolin (ROF) is a bioactive plant flavonoid with potent antioxidant and anti-inflammatory activity. However, no delivery system has yet been developed for ROF to overcome its biopharmaceutical limitations. The purpose of this study was to design a ROF-loaded polymeric nanocarrier as a potential anti-inflammatory nanomedicine. ROF was isolated from Jordanian *Teucrium polium* L. and entrapped into poly(lactide-*co*-glycolide) nanoparticles (PLGA NPs), followed by tannic acid-mediated surface modification with poly(ethylene glycol) (PEG). The optimal ROF NPs were highly monodisperse with an average diameter of 204 nm, a zeta potential of −28 mV, an entrapment efficiency of 45%, and drug loading of 9% w/w. The NPs exhibited excellent colloidal stability during storage and in the presence of serum and achieved sustained drug release for up to 96 h at physiologic (7.4) and acidic pH (5.0). *In vitro* cell-free antioxidant assays confirmed the potent radical scavenging activity of free ROF and ROF NPs. Moreover, ROF NPs were superior to free ROF in relieving oxidative stress in stimulated RAW 264.7 murine macrophages, which was attributed to enhanced cellular uptake of the NPs as confirmed by confocal microscopy and fluorimetry. *In vivo* anti-inflammatory activity was evaluated in a formalin-induced rat paw edema model. The results showed that ROF NPs were superior to free ROF in mitigating the histopathological changes in the inflamed paw tissues. Moreover, the NPs were equally potent to free ROF and the nonsteroidal anti-inflammatory drug diclofenac in terms of inhibiting the increase in paw thickness, normalizing nitric oxide levels, and modulating the gene expression of pro-inflammatory cytokines in the inflamed paw tissues. Our findings present a promising nanocarrier platform that can enhance the solubility and control the release of ROF, which will facilitate its administration in the treatment of inflammatory diseases.

Received 28th February 2022,
Accepted 28th July 2022

DOI: 10.1039/d2bm00309k

rsc.li/biomaterials-science

Introduction

Inflammation is the underlying pathological process of most human diseases and plays an essential role in host defense against pathogens.[1] The cardinal signs of inflammation include heat, swelling, redness, pain, and loss of function, which are mediated by the extravasation of leukocytes, vasodilation, and excessive release of inflammatory mediators.[2,3] The acute phase of inflammation is characterized by vascular changes along with the accumulation of fluids, neutrophils, chemokines and cytokines, followed by tissue repair. Persistent acute inflammation leads to a progressive alteration in the type of cells and released mediators, resulting in chronic inflammation. If left uncontrolled, chronic inflammation may lead to a variety of diseases such as rheumatoid arthritis (RA), cancer, asthma, inflammatory bowel disease (IBD), Parkinson's disease, and auto-immune disorders.[4] Corticosteroids and nonsteroidal anti-inflammatory drugs (NSAIDs) are the primary treatments for inflammatory disorders. However, studies have shown that their long-term use causes many adverse effects, such as cardiovascular complications, infections, diabetes, osteoporosis, and gastrointestinal ulcers and bleeding.[5–9] For this reason, it is highly desirable to develop alternative drug candidates for the treatment of inflammation.

Over the last few decades, there has been a growing interest in isolating and analyzing the bioactive constituents of medicinal plants to elucidate their health benefits, including their potential role in immunomodulation and inflammation.[10–13] Plant polyphenols are among the leading candidates as anti-inflammatory agents due to their free-radical scavenging pro-

Department of Pharmacy, Faculty of Pharmacy, Al-Zaytoonah University of Jordan, P. O. Box 130, Amman 11733, Jordan. E-mail: suhair.sunoqrot@zuj.edu.jo; Fax: +962-6-4291432; Tel: +962-6-4291511, ext. 197

†Electronic supplementary information (ESI) available: Spectral characterization of rhoifolin, survey and high-resolution XPS spectra, cell viability assays. See DOI: https://doi.org/10.1039/d2bm00309k

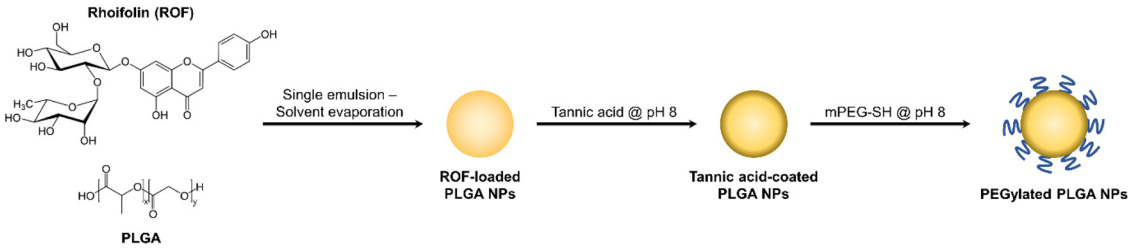

Fig. 1 An overview of the preparation of ROF-loaded PLGA NPs.

perties and their ability to modify the expression of pro-inflammatory mediators.[14,15] Rhoifolin (ROF, apigenin 7-*O*-β-neohesperidoside) (Fig. 1) is a trisubstituted flavone and a naturally occurring glycoside of apigenin. It is found in several dietary sources and edible plants such as grapefruit, bitter orange, lemon, grapes, tomatoes, and bananas.[16] Preclinical studies have shown that ROF possesses a variety of significant biological activities including anti-inflammatory,[17,18] anti-arthritic,[19] and anticancer effects.[20] However, clinical use of plant polyphenols such as ROF has been limited due to many challenges such as poor water solubility, low stability, poor bioavailability and permeability, and fast release.[21] Therefore, designing an appropriate drug delivery system is necessary to conquer those limitations.

Nanocarriers have achieved considerable steps forward in bringing anti-inflammatory phytochemicals closer to therapeutic applications.[22] Polymeric nanoparticle (NP) drug delivery systems provide a versatile paradigm for targeting inflammation because of their biocompatibility, low toxicity, and biodegradability.[23] In addition, they can enhance drug absorption because of their nanometer size and ability to permeate across biological barriers. They can protect drugs from premature enzymatic degradation, increase the stability and solubility of hydrophobic drugs, and offer sustained drug release and prolonged circulation times, which can increase patient compliance. Furthermore, they can be prepared using cost effective and scalable methods.[24–26] Poly(lactide-*co*-glycolide) (PLGA) is among the commonly used polymers for NP fabrication because of its biocompatibility, biodegradability, stability, and possibility to modify surface properties. It is also approved by the US Food and Drug Administration (FDA) for human administration.[27,28]

Despite the potent role of ROF as an anti-inflammatory agent,[17–19] like other molecules in its class, it suffers from poor aqueous solubility,[29] which can greatly hinder its clinical application. At the same time, no delivery system has yet been developed for this promising drug candidate. Thus, we hypothesized that PLGA polymeric NPs could serve as a delivery platform for ROF to overcome its biopharmaceutical challenges in therapeutic applications such as inflammation. To validate our hypothesis, ROF was first isolated from Jordanian *Teucrium polium* (germander), an herbaceous medicinal plant known to be rich in flavonoids and abundant in the Mediterranean region.[30–32] ROF was then entrapped in poly(ethylene glycol) (PEG)-modified PLGA NPs. The NPs were prepared, optimized, and characterized to determine their physicochemical properties. Then, the antioxidant and anti-inflammatory activities of the optimized NPs were evaluated *in vitro* in RAW 264.7 murine macrophages and *in vivo* in a formalin-induced rat paw edema model.

Materials and Methods

Materials

ROF was isolated from Jordanian *T. polium* (germander) as described below. PLGA (lactide/glycolide ratio 50 : 50, 5–10 kDa) and bicine were purchased from Acros Organics (USA). Poly(vinyl alcohol) (PVA, MW 13–23 kDa, 87–89% hydrolyzed), tannic acid (TA), Nile red (NR), acetic acid, and formalin (~37% in water) were purchased from Sigma-Aldrich (USA). Diclofenac deanolate (DIC, Tratul® ampoules) was obtained from Gerot Pharmazeutika (Australia). Methoxy poly(ethylene glycol)-thiol (mPEG-SH, MW 5 kDa) was purchased from Laysan Bio (USA). Dimethyl sulfoxide (DMSO), dichloromethane (DCM), and potassium bromide (KBr) were obtained from Fisher Chemicals (Thermo Fisher Scientific, UK). Phosphate buffered saline solution (PBS, 10×, pH 7.4) was purchased from Fisher Bioreagents (USA). Tween 80 was procured from RCFL Limited (India). 2,2′-Azino-bis(3-ethylbenzothiazoline-6-sulfonic acid) (ABTS diammonium salt chromogenic peroxidase substrate) was obtained from Abcam (UK). Potassium permanganate ($KMnO_4$) was purchased from Riedel-de Haën (Germany). Ultrapure water was prepared using an EMD Millipore Direct-Q 5UV system (USA).

Isolation of ROF from *T. polium*

Jordanian *T. polium* was collected, defatted, and extracted using ethanol as described in our previous publication.[33] The crude ethanolic extract was dried under vacuum and then partitioned between chloroform and water (1.1 L : 1.1 L). The water layer was extracted with 2.5 L butanol to give 264 g of butanol extract and 120 g of water extract. The butanol extract (TB, 146 g) was adsorbed on 150 g of silica gel 60 and subjected to column chromatography (62 × 7.0 cm) using 800 g of the same adsorbent. The column was packed in chloroform and the polarity was gradually increased using methanol, till pure methanol was added. Five hundred milliliter fractions (a

total of 110 fractions) were collected and grouped into six groups designated TBI–TBVI. Fraction TBVI was further treated with methanol, which led to precipitation of a yellow UV-active solid (2993 mg) that was identified as ROF. M. p.: 312 °C. HRMS (Bruker Daltonics Apex IV, 7.0 T Ultra Shield Plus) *m*/*z*: 601.15278 $[M + Na]^+$. IR (KBr; Thermo-Nicolet Nexus 870 FT-IR spectrophotometer) υ max cm^{-1}: 3275, 2904, 1654, 1602, 1586, 1495, 1344, 1292, 1180, 833. UV λ_{max} (MeOH; Shimadzu UV-1800 spectrophotometer) nm: 333 (band I), 226 (band II); + NaOMe: 391 (band I), 229 (band II); + $AlCl_3$: 387 (band I), 229 (band II); + HCl: 387 (band I), 229 (band II). ^{1}H NMR (300 MHz, DMSO-d_6) δ ppm: 3.12–5.44 (complex CH, CH_2, CH_3, diglucoside moiety), 6.42 (1H, d, J = 1.2 Hz, H-6), 6.76 (1H, d, J = 1.3 Hz, H-8), 6.83 (1H, s, H-3), 6.92 (2H, d, J = 8.6 Hz, H-3′,5′), 7.91 (2H, d, J = 8.6 Hz, H-2′,6′), 12.93 (C5–OH). ^{13}C NMR (75 MHz, DMSO-d_6) δ ppm: 18.3 (C-6‴), 66.5 (C-6″), 68.8 (C-5‴), 70.0 (C-4″), 70.8 (C-3‴), 71.2 (C-2‴), 72.5 (C-4‴), 73.6 (C-2″), 76.1 (C-5″), 76.7 (C-3″), 95.3 (C-8), 100 (C-6), 100.3 (C-1″), 101.0 (C-1‴), 103.6 (C-3), 105.9 (C-10), 116.6 (C-3′,5′), 121.5 (C-1′), 129.1 (C-2′,6′), 157.4 (C-9), 161.7 (C-4′), 161.9 (C-5), 163.3 (C-7), 164.8 (C-2), 182.5 (C-4). Spectral characterization of ROF is presented in the ESI.†

Preparation of ROF-loaded PEGylated PLGA NPs

Preparation of ROF-loaded PLGA NPs. In this study, PLGA NPs loaded with ROF were prepared by the single emulsion (O/W) solvent evaporation technique according to a previous study with some modification.[34] Briefly, 10–50 mg of PLGA and 2.5–10.0 mg of ROF (from a stock solution in DMSO) were dissolved in 1 mL DCM to obtain a clear solution. The organic phase was emulsified with the aqueous phase consisting of 3% w/v PVA solution (4 mL) using an ultrasonic homogenizer (Omni Sonic Ruptor 400, Omni International, USA). Sonication was performed in a 50 mL glass vial immersed in an ice bath at 70 W and 80% power for 1 min. The resulting O/W emulsion was quickly poured into 16 mL of 0.3% w/v PVA aqueous solution and kept under magnetic stirring overnight at room temperature to allow complete evaporation of DCM. The obtained NP suspension was centrifuged (Hermle Z326K centrifuge, Germany) at 10 000*g* for 40 min at 4 °C and washed with water to remove trace DMSO, PVA, and unentrapped drug. The supernatant was collected, and the NP pellet was resuspended in ultrapure water under sonication (Elmasonic S 40-H, Germany) and stored at 4 °C. For the preparation of NR-labeled PLGA NPs, ROF was replaced with 0.5 mg NR and the NPs were prepared using 50 mg PLGA as described above.

PEGylation of ROF-loaded PLGA NPs

The optimal NP formulation was chosen based on drug loading efficiency and coated with TA as an adhesive layer to facilitate PEGylation as previously reported.[35] Briefly, NPs were suspended in 2 mL bicine buffer (0.1 M, pH 8) containing 1 mg mL^{-1} of TA and incubated for 30 min under sonication (Elmasonic S 40-H), then for 90 min under vigorous stirring. The NP dispersion was then centrifuged at 10 000*g* for 40 min at 4 °C and washed with water to remove excess bicine and TA. The supernatant was discarded, and the NP pellets were collected and called PLGA@TA NPs. For PEGylation, PLGA@TA NPs were conjugated with mPEG-SH by relying on the reactivity of oxidized TA toward nucleophiles as previously described.[36] Briefly, NPs were resuspended in 2 mL bicine buffer (0.1 M, pH 8) containing 50 mg mPEG-SH and incubated for 30 min under sonication (Elmasonic S 40-H) and then for 90 min under vigorous stirring. The NP dispersion was then centrifuged at 10 000*g* for 40 min at 4 °C and washed with water to remove excess bicine and mPEG-SH. The supernatant was discarded, and the NP pellets were collected, resuspended in ultrapure water under sonication (Elmasonic S 40-H), stored at 4 °C, and called PLGA@PEG NPs (ROF NPs). NR-labeled PLGA NPs were also primed with TA and PEGylated as described above for ROF NPs.

Particle size and zeta potential analysis

The particle size and polydispersity index (PDI) of the prepared NPs were measured by dynamic light scattering (DLS). Freshly prepared NPs were diluted appropriately with ultrapure water and the measurements were acquired using a Nicomp® Nano Z3000 particle sizing system (Entegris, USA). Zeta potential was measured *via* electrophoretic light scattering using the same instrument in the zeta potential mode. Measurements were reported as the mean ± standard deviation (SD) from at least three different NP batches.

Entrapment efficiency (EE) and drug loading (DL) determination

The entrapment efficiency of ROF in the various batches of PLGA NPs was determined indirectly by analyzing the supernatant from the first centrifugation step by UV-Vis (UV-1800 spectrophotometer, Shimadzu, Japan). A calibration curve of ROF absorbance at 340 nm *versus* concentration in DMSO was constructed to determine the amount of unentrapped drug in the supernatant. EE and DL were calculated according to eqn (1) and (2), respectively, as follows:

$$\mathrm{EE}\,(\%) = \frac{\text{Theoretical amount of ROF (mg)} - \text{Amount of unentrapped ROF (mg)}}{\text{Theoretical amount of ROF (mg)}} \times 100\% \quad (1)$$

$$\mathrm{DL}\,(\%) = \frac{\text{Theoretical amount of ROF (mg)} - \text{Amount of unentrapped ROF (mg)}}{\text{Amount of PLGA (mg)}} \times 100\% \quad (2)$$

The amount of NR entrapped in NR-labeled NPs was calculated as described above for ROF, except that the UV absorbance of the supernatant was measured at 552 nm.

Fourier transform-infrared (FTIR) spectroscopy

ROF NPs were lyophilized using a freeze dryer system (FreeZone 4.5 L benchtop freeze dryer, Labconco, USA) at

−50 °C and 0.5 mbar and prepared as KBr pellets. FTIR spectra of free ROF and ROF NPs were recorded using a Shimadzu IR Affinity-1 spectrometer (Japan) with data scanning from 4500 to 650 cm^{-1}.

X-ray photoelectron spectroscopy (XPS)

XPS was carried out to verify surface modification of ROF NPs. Freshly prepared PLGA, PLGA@TA, and PLGA@PEG NPs (ROF NPs) were each resuspended in 100 μL ultrapure water and drop-casted on pre-cleaned TiO_2-coated Si wafers. The wafers were dried under vacuum and analyzed using a Kratos Axis SUPRA instrument fitted with a monochromated Al Kα X-ray source (1486.7 eV). All data was recorded at 150 W and a spot size of 700 × 300 μm. Survey scans and high-resolution scans were recorded at 160 eV and 20 eV pass energies, respectively. Electronic charge neutralization was achieved using a magnetic immersion lens. Data was analyzed using CasaXPS v2.3.20PR1.0 and the spectra were calibrated by setting the C 1s peak at 284.8 eV.

Transmission electron microscopy (TEM)

ROF NPs were observed using TEM (Morgagni 268D, FEI, Netherlands) at an accelerating voltage of 60 kV. A drop of the NP dispersion was placed on a Formvar-coated copper grid (300 mesh, Electron Microscopy Sciences, USA) for 1 min, and the excess was wicked with filter paper. The grid was kept at room temperature overnight to air dry prior to imaging.

Stability of ROF NPs

Storage stability of ROF NPs was evaluated by tracking the change in particle size up to 4 months of storage at 4 °C. Stability was also evaluated by incubating freshly prepared NPs in Dulbecco's Modified Eagle's Medium (DMEM, Euroclone, Italy) supplemented with 10% fetal bovine serum (FBS; Capricorn, Germany) at 37 °C under shaking at 100 rpm (Biosan ES-20 Orbital Shaker-Incubator, Latvia), withdrawing samples every 24 h up to 96 h to measure the size. Fold increase in size relative to fresh NPs was calculated from the ratio of particle size after storage or incubation to the particle size of freshly prepared NPs. Each experiment was performed in triplicate.

In vitro release of ROF from loaded NPs

ROF release was conducted by the centrifugation method.[37] Pellets of ROF NPs were suspended in 2 mL of phosphate buffered saline (PBS, pH 7.4) or acetate buffer (pH 5.0) containing 0.5% w/v Tween 80 to solubilize the released ROF. Experiments were performed in triplicate in 2 mL microtubes. The tubes were placed in a shaking incubator (Biosan ES-20 Orbital Shaker-Incubator) operating at 37 °C and 100 rpm. At predetermined time intervals (1, 2, 4, 6, 24, 48, 72, and 96 h), NP dispersions were centrifuged at 10 000*g* for 30 min to separate the released ROF from the NPs. After centrifugation, 500 μL of the supernatant was withdrawn and replaced with an equal amount of fresh PBS. The precipitated pellets in each tube were redispersed and incubated until the next sampling point. The amount of released ROF in the supernatant was determined by UV-Vis at 340 nm, based on a calibration curve of ROF in the release medium. The percentage of cumulative release was calculated from the ratio of the cumulative amount of ROF released at each time interval to the total amount of ROF entrapped in the NPs. Cumulative release (%) of ROF was then plotted against time (h) to obtain the release profile.

In vitro antioxidant activity of ROF NPs

Antioxidant activity of ROF and ROF NPs was determined using the ABTS assay following a previously described method.[38] Briefly, the ABTS radical was produced by reacting the ABTS salt (3.6 mM in water) with $KMnO_4$ solution (2.4 mM in water) in the dark for 18 h under stirring at room temperature. The produced blue-green solution was diluted ten times with ultrapure water to give an absorbance of 0.7 at 734 nm. Different amounts (1.25–200 μg) of ROF as free drug or an equivalent amount of ROF NPs were dissolved in 200 μL DMSO (the NPs were incubated overnight in DMSO to ensure complete breakdown and release of ROF). After adding 1 mL of diluted ABTS solution to 200 μL of each sample, samples were incubated at room temperature for 30 min in the dark, and the absorbance (Abs.) was measured at 734 nm. Solvent blanks (1 mL ABTS + 200 μL DMSO) were also run in each assay. The experiment was performed in triplicate. Scavenging activity (%) was calculated according to eqn (3):

$$\text{Scavenging activity}\,(\%) = \frac{\text{Abs. of blank} - \text{Abs. of sample}}{\text{Abs. of blank}} \times 100\% \quad (3)$$

Antioxidant activity of ROF NPs in RAW 264.7 murine macrophages

Cell culture. The RAW 264.7 cell line was obtained from the American Type Culture Collection (ATCC, USA). Cells were maintained at 37 °C in a 5% CO_2 atmosphere in DMEM supplemented with 10% FBS and penicillin–streptomycin (100 U mL^{-1}–100 μg mL^{-1}, Euroclone, Italy).

Cell viability assay

When the cells reached 80% confluence, they were removed from the flask using a cell scraper and the cell suspension was counted. Cells were seeded in 96-well plates at a density of 10 000 cells per well and allowed to attach overnight. Then, cells (n = 5) were incubated with various concentrations of ROF and ROF NPs (0–300 μM) diluted in complete culture medium for 24 h. After 24 h, the media was completely removed and replaced with 100 μL of fresh culture medium containing 0.5 mg mL^{-1} 3-(4,5-dimethylthiazolyl-2)-2,5-diphenyltetrazolium bromide (MTT, Sigma-Aldrich, USA). Cells were incubated for another 2 h (37 °C, 5% CO_2), after which the media was carefully removed and replaced with 100 μL of DMSO to dissolve the formazan crystals. The absorbance of the plates was measured at 540 nm using a Synergy HTX multi-mode micro-

plate reader (Biotek, USA). Cell viability was determined relative to untreated cells.

Measurement of intracellular reactive oxygen species (ROS). After determining the least toxic concentration range for ROF and ROF NPs, antioxidant activity was assessed in RAW 264.7 cells by measuring intracellular reactive oxygen species (ROS) levels using 2′,7′-dichlorodihydrofluorescein diacetate (DCFDA, Abcam, UK). DCFDA diffuses into the cells, where it is cleaved by cellular esterases and oxidized by ROS into 2′,7′-dichlorofluorescein (DCF) which exhibits strong green fluorescence.[39] For the assay, cells (n = 3) were seeded in 24-well plates at a density of 50 000 cells per well and allowed to attach overnight. Then, cells were treated with ROF and ROF NPs (0–40 μM) for 24 h. After 24 h, the wells were gently washed with PBS, followed by adding 500 μL of PBS containing 20 μM DCFDA and 50 μM *tert*-butyl hydroperoxide (*t*BHP) to stimulate the cells to produce ROS.[40] After incubation with DCFDA/*t*BHP for 45 min, the fluorescence of each well was read using a Synergy HTX multi-mode microplate reader at 460 nm excitation and 528 nm emission wavelengths. Antioxidant activity was expressed as the fold increase in DCF fluorescence relative to untreated/unstimulated cells.

Cellular uptake of NR-labeled NPs

RAW 264.7 macrophages were treated with NR-labeled NPs to enable the visualization and quantification of the NPs' cellular uptake. For imaging by confocal laser scanning microscopy (CLSM), cells were seeded in 4-well chamber slides (Nunc Lab-Tek II, Thermofisher, USA) at 50 000 cells per well and allowed to attach overnight. Cells were then treated with free NR or NR-labeled NPs diluted in complete culture medium at a concentration equivalent to 1 μg mL^{-1} NR for 1 h. Another group of cells was treated with the complete culture medium alone. After 1 h, the media was removed from the wells and the cells were washed with PBS three times. After the third wash, cells were fixed in 4% paraformaldehyde for 10 min at room temperature protected from light, followed by washing with PBS. After removing the remaining PBS, the chamber gasket was detached and the slide was mounted with ProLong™ Diamond Antifade Mountant with DAPI (Invitrogen, Thermofisher, USA) and covered with a glass coverslip. Imaging was performed using a Zeiss confocal LSM 780 (Zeiss, Germany). DAPI was detected at 405 nm excitation and 410–585 nm emission wavelengths, whereas NR was detected at 561 nm excitation and 566–691 emission wavelengths. Images were acquired using a Plan-Apochromat 63×/1.4 objective at a box size of 1912 × 1912 pixels and a pixel time of 3.38 μs.

For quantification of cellular uptake by fluorimetry, cells were seeded in 24-well plates at 50 000 cells per well in triplicate and allowed to attach overnight. The next day, cells were treated with free NR or NR-labeled NPs as described above for CLSM imaging. After the treatment, the cells were washed with PBS three times, 500 μL PBS was added to each well, and NR fluorescence was measured using a Synergy HTX multi-mode microplate reader at 540 nm excitation and 620 nm emission wavelengths. Results were expressed as the average fold increase in fluorescence relative to untreated cells.

In vivo anti-inflammatory activity of ROF NPs

Animals and experimental design. All animal experiments were approved by Al-Zaytoonah University of Jordan Institutional Review Board (IRB) decision no. 1/2/2020-2021. Forty-five healthy male Wistar rats (180–250 g) were housed in the animal house, Faculty of Pharmacy, Al-Zaytoonah University of Jordan, Amman, Jordan. Animals were kept in polypropylene rat cages and maintained under standard conditions with free access to food and water. Animal welfare was taken into consideration, in accordance with the ethical guidelines of the Animal Welfare Committee of the University. All experiments were conducted in accordance with the Helsinki guidelines for animal research. Rats were divided into five groups, assigned Latin numbers I–V, and nine animals were used in each group (one animal per group for histological analysis, three animals for nitric oxide (NO) determination, and five animals for gene expression analysis).

Assessment of formalin-induced paw edema. ROF and ROF NPs were tested for anti-inflammatory activity using the formalin-induced rat paw edema model as described earlier with some modification.[41] Table 1 shows the details of the animal groups and the administered treatments. Animals in group I and II received intraperitoneal (IP) normal saline injections. Treatments were administered to groups III–V one hour before formalin injection. Animals in group III were pretreated with a 10 mg kg^{-1} IP dose of DIC as a reference anti-inflammatory drug. Animals in group IV were pretreated with a 10 mg kg^{-1} IP dose of free ROF suspended in normal saline from a 100 mg mL^{-1} stock solution in DMSO. Animals in group V were pretreated with a 10 mg kg^{-1} IP dose of an aqueous dispersion of ROF NPs diluted in normal saline. One hour after the injections, groups II–V received 0.5 mL kg^{-1} formalin (5% solution in normal saline) subcutaneously (SC) on the sub plantar surface of the right hind paw to induce paw edema. The doses used were chosen according to pilot studies in our laboratory and based on previous studies.[17–19] Note that the 10 mg kg^{-1} dose of ROF was used because the high dose (20 mg kg^{-1}) and low dose (10 mg kg^{-1}) showed similar inhibitory effects on the increase in paw thickness over a 24 h period in the pilot study. Paw thickness was measured using a digital Vernier caliper at several time points (0, 1, 2, 3, 4, 5 and 24 h post formalin injection). The caliper was placed at the border of the metatarsals and phalanges and it was just touching the ventral and dorsal surface of the hind paw. The paw thickness measured after each time point was divided by the paw thickness at the 0 h time point to obtain the fold increase in paw thickness, which

Table 1 Animal groups and treatments

	Group	Pretreatment	Inflammation induction
I	Control	IP normal saline	—
II	Untreated	IP normal saline	0.5 mL kg^{-1} SC formalin
III	DIC	10 mg kg^{-1} IP DIC	0.5 mL kg^{-1} SC formalin
IV	ROF	10 mg kg^{-1} IP free ROF	0.5 mL kg^{-1} SC formalin
V	ROF NPs	10 mg kg^{-1} IP ROF NPs	0.5 mL kg^{-1} SC formalin

was used as an indication of edema formation and the degree of inflammation. After 24 h, animals were euthanized by diethyl ether followed by cervical dislocation. Rat paws were incised with a scalpel, and either immediately placed in 10% formalin for histological analysis or snap-frozen in liquid nitrogen and stored at −80 °C for all other analyses.

Histological examination of paw tissues. For histological examination, biopsies from the paw tissues of the different animal groups were collected, fixed in 10% formalin, embedded in paraffin, sectioned, and stained with hematoxylin and eosin (H & E). Samples were interpreted by a pathologist (Alpha Medical Labs Pathology Consultations Center, Amman, Jordan) and representative images were acquired using a Primovert inverted microscope (Zeiss, Germany) equipped with an Axiocam ERc 5s digital camera at 20× magnification.

Nitric oxide (NO) assay. Oxidative stress associated with paw edema formation and the various treatments was evaluated by a nitric oxide (NO) assay. NO levels were measured indirectly by measuring the concentration of nitrite in paw tissues using the Griess assay as previously described.[42] Briefly, paw tissues were separated from the dissected paws using surgical scissors. Tissue samples were then placed in microtubes and cut into smaller pieces, followed by adding 1 mL lysis buffer. Samples were homogenized using a manual tissue homogenizer, and then placed in an ultrasonic water bath for 30 min over ice. The homogenized tissue samples were centrifuged to remove debris, and 50 μL of each sample was mixed with an equal volume of freshly prepared Griess reagent (Sigma-Aldrich, USA) in 96-well plates and incubated for 30 min at room temperature protected from light. Sodium nitrite standards (Sigma-Aldrich, USA) were also prepared in the same plate and incubated with the Griess reagent. The absorbance of the samples was then read at 540 nm using a Synergy HTX multi-mode microplate reader. The nitrite concentration in each sample was calculated based on a calibration curve of sodium nitrite standards.

RNA extraction from paw tissues and complementary DNA (cDNA) synthesis. Tissue samples were separated from dissected rat paws using surgical scissors. Total RNA was extracted from paw tissue samples using a Direct-zol RNA Miniprep kit (Zymo Research, USA) according to the manufacturer's instructions. Briefly, tissues were homogenized in 600 μL TRIzol reagent using bashing beads, centrifuged to remove debris, and the supernatants were transferred into Zymo-Spin columns in a collection tube. Columns were then treated with DNase I and DNA digestion buffer and washed with RNA prewash and RNA wash buffer. RNA samples were eluted from columns with 50 μL DNase/RNase-free water by centrifugation and RNA concentrations were analyzed using a Nanodrop DNA/Protein Analyzer (Quawell, USA). Double-stranded cDNA was synthesized from the total RNA using a Prime-Script Reverse Transcriptase (RT) Master mix (Takara Bio cDNA synthesis kit, cat# RR036A-1, Japan) in a DNA Engine® Peltier Thermal Cycler (Bio-Rad, USA). For cDNA synthesis, the total reaction volume was 10 μL consisting of 2 μL of RNA samples, 2 μL of RT, and 6 μL of nuclease-free water. cDNA sample concentrations were measured by a Nanodrop DNA/Protein Analyzer (Quawell) and were diluted with nuclease-free water (80–100 ng μL^{-1}).

Assessment of tnf-α and il-1β gene expression using reverse transcriptase-polymerase chain reaction (RT-PCR). RT-PCR for the pro-inflammatory mediators' genes (tnf-α and il-1β) was performed using SYBR green detection (TB Green Premix Ex Taq II, Takara Bio, Japan) in a Prime Pro 48 Real-time PCR machine (Cole-Parmer, UK). For quantitative RT-PCR of tnf-α and il-1β, the total reaction volume was 20 μL consisting of 1 μL of diluted cDNA samples, 1 μL of each forward primer (FW), 1 μL of each reverse primer (RW), 10 μL SYBR green, and 7 μL nuclease-free water. Sequences of primer pairs for each pro-inflammatory mediator genes used in the analysis were previously described[43] and listed in Table 2. β-actin was used as a housekeeping gene standard in all experiments. The $2^{-\Delta\Delta C_T}$ method[44] was used to compare the relative amount of target mRNA in the untreated, DIC, ROF and ROF NPs groups with those of the control group using a threshold cycle number (C_T) for each sample obtained from an iCycler (Bio-Rad, Germany). Each sample was run in triplicate. In order to calculate ΔC_T, the mean C_T value for the internal control gene (β-actin) was subtracted from the mean C_T value of the gene of interest (tnf-α or il-1β). The average ΔC_T values of the control group was then subtracted from each ΔC_T value of the untreated, DIC, ROF, and ROF NPs groups to obtain $\Delta\Delta C_T$. The relative fold changes from the control were then expressed by calculating $2^{-\Delta\Delta C_T}$ for each sample.

Statistical analysis

Experimental results were expressed as mean ± SD from at least three independent trials. All statistical analyses were performed in GraphPad Prism 7 software. Unless otherwise indicated, means were compared using one-way analysis of variance (ANOVA) followed by Tukey's multiple comparisons test, or two-way ANOVA followed by Sidak's multiple comparisons test to determine significant differences between groups. Values of $p < 0.05$ were considered statistically significant.

Results

Isolation of ROF from *T. polium* and spectral characterization

The spectroscopic data for ROF is presented in the ESI.† The IR spectrum of the compound (Fig. S1†) showed absorption

Table 2 Genes and primer sequences used in RT-PCR[43]

Gene	Primer	Sequence (5′–3′)
tnf-α	Forward	AAATGGGCTCCCTCTCATCAGTTC
	Reverse	TCTGCTTGGTGGTTTGCTACGAC
il-1β	Forward	CACCTCTCAAGCAGAGCACAG
	Reverse	GGGTTCCATGGTGAAGTCAAC
β-actin	Forward	AAGTCCCTCACCCTCCCAAAAG
	Reverse	AAGCAATGCTGTCACCTTCCC

bands at 1602 and 1586 cm^{-1} for the aromatic rings of the flavone, and at 3275 and 1654 cm^{-1} which are characteristic of –OH and –C═O groups, respectively. High-resolution mass spectrometry (HRMS) of the compound (Fig. S2†) showed a peak at *m*/*z* 601.15278, which belongs to the $[M + Na]^+$ ion. The UV/Vis spectra of the compound in methanol showed two maxima, at 333 nm and 226 nm for band I and band II, respectively. Addition of NaOMe led to a bathochromic shift of 58 nm without the appearance of a new band, indicating the presence of free –OH at C-4′ and the absence of –OH at C-7. The presence of free –OH on C-5 was indicated by a bathochromic shift of 54 nm in $AlCl_3$. The shift was not affected by the addition of HCl, justifying the absence of *ortho* dihydroxy substitution of ring B. The ^1H and ^{13}C NMR spectra showed signals corresponding to apigenin and two sugar moieties. The ^1H NMR (DMSO-d_6) spectrum (Fig. S3†) showed two doublet peaks each integrating to one proton at 6.41 and 6.74 ppm (J = 1.9 Hz) due to the *meta* coupled protons on ring A (H-8 and H-6, respectively). H-3 appeared as a singlet at 6.83 ppm. The presence of the *para* substituted B ring was indicated by the two doublet peaks each integrating to 2 protons at 6.92 and 7.91 ppm (J = 8.7 Hz), referring to H-3′,5′ and H-2′,6′, respectively. The presence of rhamnose in the sugar moiety was indicated by the three protons doublet at 1.03 ppm for the methyl group. The β-linkage of the diglucoside was confirmed by the high value of coupling constant of the two anomeric protons, which appeared at 3.80 ppm (J = 10.8 Hz) and 5.03 ppm (J = 7.0 Hz), which correspond to H‴ and H″, respectively. The ^{13}C NMR (DMSO-d_6) spectrum (Fig. S4†) and the DEPT experiment of the compound (Fig. S5†) showed the presence of 25 carbon signals corresponding to 27 carbons, classified as one $–CH_3$, one $–CH_2$, 17 –CH, and 8 quaternary carbons. Thirteen of the C-signals are due to the apigenin moiety, and the remaining 12 C-signals are due to the sugar moiety. The spectral data of ROF were in full agreement with literature values.[45]

Preparation and characterization of ROF-loaded PLGA NPs

Optimization of ROF loading. An overview of the preparation of ROF-loaded PLGA NPs is depicted in Fig. 1. Several methods have been used for the preparation of polymeric NPs.[46] In this study, the single emulsion/solvent evaporation method was successfully used to entrap ROF in PLGA NPs. Various formulations were prepared that mainly differed in the amount of PLGA used and the ROF : PLGA ratio (Table 3). All NPs exhibited a particle size between 150–260 nm with relatively low polydispersities. Entrapment efficiency (EE%) and drug loading (DL%) were used to determine the percentage amount of drug successfully entrapped into the NPs. ROF-loaded NPs prepared at different ROF : PLGA ratio showed an EE% ranging between 26.3% and 45.0% and a DL% ranging between 1.4% and 9.0%. It was observed that the EE increased with the increase in both PLGA and ROF amounts. The highest EE of 45.0% was obtained for formulation NP3 containing the highest amounts of ROF and PLGA (10 mg and 50 mg, respectively). It was also observed that DL increased proportionally with the increase in the amount of ROF added. For example, when a constant amount of 50 mg PLGA was maintained, DL increased from 2.0% to 9.0% upon increasing the amount of ROF from 2.5 mg to 10 mg. Also, when a constant amount of 20 mg PLGA was maintained, DL was increased from 1.8% to 5.4% as the amount of ROF was increased from 1 mg to 4 mg. Similarly, when a constant amount of 10 mg PLGA was maintained, DL was increased from 1.4% to 5.3% by increasing the amount of drug from 0.5 mg to 2 mg. These findings may be explained based on the change in viscosity of the emulsion produced during preparation of the NPs. For example, increasing the amount of PLGA increased the viscosity of the organic phase, resulting in high resistance to diffusion of ROF from the organic phase to the aqueous phase, thereby encapsulating more ROF in the PLGA NPs. Furthermore, increased ROF amount in the organic phase led to an increase in EE% and DL% which may be due to the more available ROF molecules that could interact with the PLGA polymer chains.[47] The particle size of all NP formulations as measured by DLS ranged between 153 and 263 nm, with PDI values ranging between 0.14 and 0.25 (Table 3), denoting narrow particle size distributions. Based on the EE and DL results, NP3 was chosen for further investigation.

Surface modification of ROF NPs. ROF-loaded PLGA NPs that exhibited the highest EE and DL (NP3) were PEGylated to provide steric stabilization and stealth properties.[48] This was achieved by priming the NPs with a plant-inspired TA coating as an adhesive layer to facilitate PEGylation. TA is a complex plant polyphenol which has been reported to form reactive adhesive coatings on various organic and inorganic substrates

Table 3 Characterization of the different formulations of ROF-loaded PLGA NPs

NP	PLGA (mg)	ROF (mg)	Particle size (nm)	PDI	EE (%)	DL (%)
NP1	50	2.5	168 ± 16	0.19 ± 0.02	39.8 ± 16.5	2.0 ± 0.8
NP2	50	5	181 ± 24	0.19 ± 0.01	36.1 ± 21.7	3.6 ± 2.2
NP3	50	10	182 ± 8	0.15 ± 0.01	45.0 ± 4.3	9.0 ± 0.9
NP4	20	1	153 ± 17	0.25 ± 0.09	35.8 ± 4.9	1.8 ± 0.2
NP5	20	2	178 ± 47	0.21 ± 0.05	31.8 ± 12.6	3.2 ± 1.3
NP6	20	4	223 ± 17	0.23 ± 0.11	27.2 ± 13.6	5.4 ± 2.7
NP7	10	0.5	213 ± 66	0.19 ± 0.06	28.9 ± 12.5	1.4 ± 0.6
NP8	10	1	263 ± 27	0.22 ± 0.13	37.0 ± 22.1	3.7 ± 2.2
NP9	10	2	255 ± 38	0.18 ± 0.01	26.3 ± 8.7	5.3 ± 1.7

upon oxidation in mild alkaline buffers.[49] These coatings can be conveniently exploited to immobilize nucleophilic ligands such as thiol-terminated PEG (mPEG-SH).[35,36] Thus, PEG was immobilized on the surface of the ROF-loaded, TA-coated PLGA NPs (PLGA@TA NPs), producing the optimized ROF formulation (PLGA@PEG NPs; ROF NPs). As shown in Table 4, the particle size and polydispersity of ROF-loaded uncoated PLGA NPs (NP3) did not significantly change upon TA coating and PEGylation, averaging a diameter of 204 nm and a PDI of 0.14. Uncoated PLGA NPs (NP3) and PLGA@TA NPs exhibited a partially negative surface charge (zeta potential values of −27 and −30 mV, respectively) due to the presence of terminal carboxyl groups and terminal galloyl groups, respectively. After PEGylation, the surface charge of PLGA@PEG NPs was not significantly decreased, most likely due to the persistence of carboxyl and galloyl groups near the NP surface.

XPS was employed to verify successful PEGylation of ROF NPs by comparing the surface chemistry of uncoated PLGA, PLGA@TA, and PLGA@PEG NPs. XPS survey and high-resolution scans of the NPs before and after PEGylation are provided in the ESI,† and the relative composition of the C 1s peak components is depicted in Table 5. Uncoated PLGA NPs produced a C/O ratio of 1.05, which is lower than the theoretical value for PLGA of 1.25. This was most likely attributed to the presence of extra oxygens arising from incomplete removal of PVA during NP preparation and/or surface exposed ROF molecules. On the other hand, PLGA@TA NPs exhibited an increase in the C/O ratio to 1.70, which is close to the theoretical value for TA of 1.65. The increase in the C/O ratio was accompanied by an increase in the % of the C–C/C–H components from 54.2 to 66.0%, and a decrease in the % of the C═O component from 21.8 to 10.3%, confirming successful TA coating. PEGylation resulted in further changes to the NPs' surface chemistry. Notably, PLGA@PEG NPs showed a decrease in the C/O ratio from 1.70 to 1.04, reflecting a rise in the % of oxygen species on the NP surface. Additionally, there was a marked decrease in the % of the C–C/C–H components from 66.0 to 34.6% and an increase in the % of the C–O/C–OH components from 23.7 to 42.6%. These changes strongly support the successful immobilization of PEG on the NPs' surface mediated by the TA adhesive layer, as a facile surface modification approach to produce sterically stabilized ROF NPs.

Physicochemical characterization of ROF NPs. The optimized ROF NPs were characterized by FTIR. As shown in Fig. 2A, the FTIR spectra of ROF and the optimized ROF NPs both showed characteristic O–H stretching bands between 3100–3700 cm^{-1} and C–H stretching bands between 2800–3000 cm^{-1}. The C═O stretching band observed in ROF NPs between 1650–1750 cm^{-1} was assigned to the ester groups of PLGA, and the C–O stretching bands appearing in both ROF and ROF NPs were attributed to the multiple C–OH groups in ROF and the ethylene oxide units of PEG, respectively. The NPs were further examined using TEM, which confirmed their spherical morphology with an approximate diameter of 110 nm (Fig. 2B). Note that particle diameters measured from electron microscopy images are typically smaller than DLS readings due to the collapsed state of the NPs under vacuum during TEM imaging.[38] The colloidal stability of ROF NPs upon storage at 4 °C was evaluated by measuring the change in particle size over time. As shown in Fig. 2C, there was no significant increase in size up to 4 months compared to freshly prepared NPs. Serum stability of NPs is also crucial, since small particles may react with different blood components and aggregate during systemic administration. To examine the serum stability of ROF NPs, the fresh NP dispersion was incubated in DMEM supplemented with 10% FBS at 37 °C, withdrawing samples every 24 h up to 96 h. As shown in Fig. 2C, there was no statistical difference in terms of fold increase in size compared to freshly prepared NPs.

Sustained release from the drug delivery system is a desirable property to maintain a constant therapeutic concentration of the drug for a prolonged period of time. Therefore, *in vitro* release of ROF from the optimized ROF NPs was investigated in PBS pH 7.4 at 37 °C to mimic physiologic conditions. Release was also conducted in acetate buffer pH 5.0 to examine the effect of pH on modulating drug release. As shown in Fig. 2D, under both pH conditions, the release behavior of ROF from the NPs followed a biphasic pattern, where an initial fast release was observed during the first 6 h, followed by a slower sustained release pattern over 96 h. In PBS pH 7.4, approximately 54.3% of ROF was released from the NPs within the first 6 h, 80.2% was released after 24 h, 90.8% was released after 48 h, 97.6% was released after 72 h, and

Table 4 Characterization of ROF NPs before and after PEGylation

NP	Particle size (nm)	PDI	Zeta potential (mV)
PLGA NPs (NP3)	182 ± 8	0.15 ± 0.01	−27 ± 8
PLGA@TA NPs	197 ± 4	0.16 ± 0.01	−30 ± 4
PLGA@PEG NPs (ROF NPs)	204 ± 2	0.14 ± 0.02	−28 ± 3

Table 5 Relative composition of the C and O components of ROF NPs before and after PEGylation obtained from XPS

	Atomic composition (%)			Composition of C 1s components (%)		
NP	C 1s	O 1s	C/O	C–C/C–H	C–O/C–OH	C═O
PLGA	51.2	48.8	1.05	54.2	24.0	21.8
PLGA@TA	63.0	37.0	1.70	66.0	23.7	10.3
PLGA@PEG	50.9	49.1	1.04	34.6	42.6	22.8

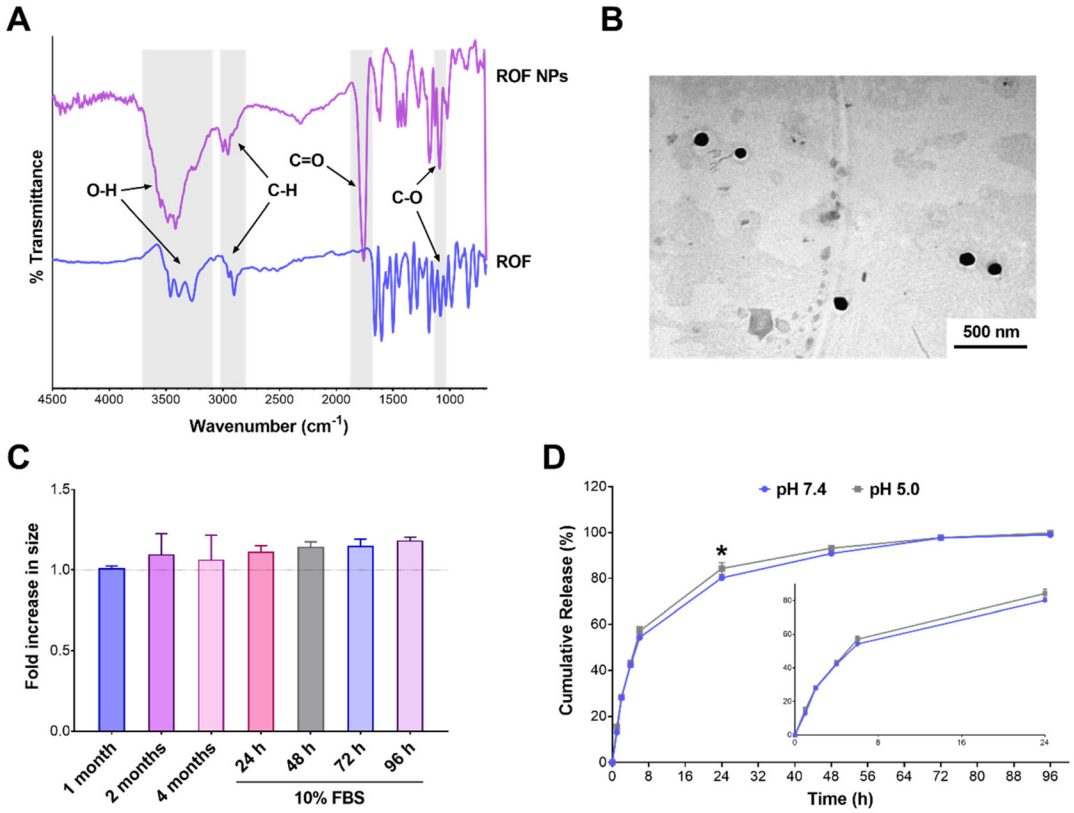

Fig. 2 (A) FTIR spectra of ROF and the optimized ROF NPs; (B) TEM image of the optimized ROF NPs; (C) Colloidal stability of the optimized ROF NPs upon storage up to 4 months at 4 °C and after incubation in DMEM supplemented with 10% FBS up to 96 h at 37 °C. Results are expressed as the average fold increase in size ± SD relative to fresh NPs (n = 3); (D) *In vitro* release of ROF from the optimized ROF NPs in PBS pH 7.4 and acetate buffer pH 5.0 at 37 °C. Results are expressed as the average % cumulative release ± SD (n = 3) *versus* time. *p < 0.05 based on two-way ANOVA followed by Sidak's multiple comparisons test.

99.0% was released after 96 h. Release in acetate buffer pH 5.0 followed similar kinetics, except that 84.3% of ROF was released at 24 h, which was significantly higher than the amount released in PBS pH 7.4 (p < 0.05). No differences were observed at all the other time points, reflecting the slow degradation rate of PLGA and indicating that drug release was mainly governed by diffusion.[50]

Antioxidant activity of ROF NPs

The antioxidant and anti-inflammatory properties of polyphenols have been largely attributed to their chemical structures. The highly conjugated aromatic system with multiple hydroxyl groups makes these compounds good hydrogen donors or electron donors, neutralizing free radicals and other reactive species.[51] The antioxidant activity of the optimized ROF NPs was compared to free ROF using the ABTS assay. Different amounts of ROF and ROF NPs were incubated with the ABTS radical solution, and the decrease in absorbance of the ABTS radical was used as an indication of the radical scavenging activity. As shown in Fig. 3A, ROF NPs exhibited a dose-dependent increase in scavenging activity which was comparable to free ROF, indicating that the antioxidant activity of free ROF was not compromised during NP preparation.

The antioxidant and free radical scavenging activity of ROF NPs was further evaluated in a cell-based assay using RAW 264.7 macrophages. Cells were first treated with various concentrations of free ROF and ROF NPs for 24 h and cell viability was determined (Fig. S8†). Then, cells were treated with non-toxic concentrations of free ROF or ROF NPs for 24 h, followed by inducing oxidative stress using a hydrogen peroxide derivative, *t*BHP, and monitoring the extent of cellular ROS generated as indicated by the fluorescence signal of the DCFDA probe. Interestingly, even though ROF in its free and NP form exhibited similar antioxidant activities in the cell-free assay (Fig. 3A), the two forms showed different behaviors in the cell-based assay. As depicted in Fig. 3B, *t*BHP caused a significant increase in cellular ROS in untreated/stimulated cells. Pretreating the cells with free ROF before *t*BHP stimulation did not have a significant effect on the elevated ROS levels even at the highest ROF concentration (40 μM). Conversely, cells pretreated with 10 and 20 μM ROF NPs maintained a cellular ROS level that was similar to that of untreated/unstimulated control cells. Moreover, at 40 μM, ROF NPs were associated with a significant reduction (p < 0.0001) in the cellular ROS level compared to the untreated/unstimulated controls, denoting their ability to reduce intrinsic oxidative stress. Additionally, the

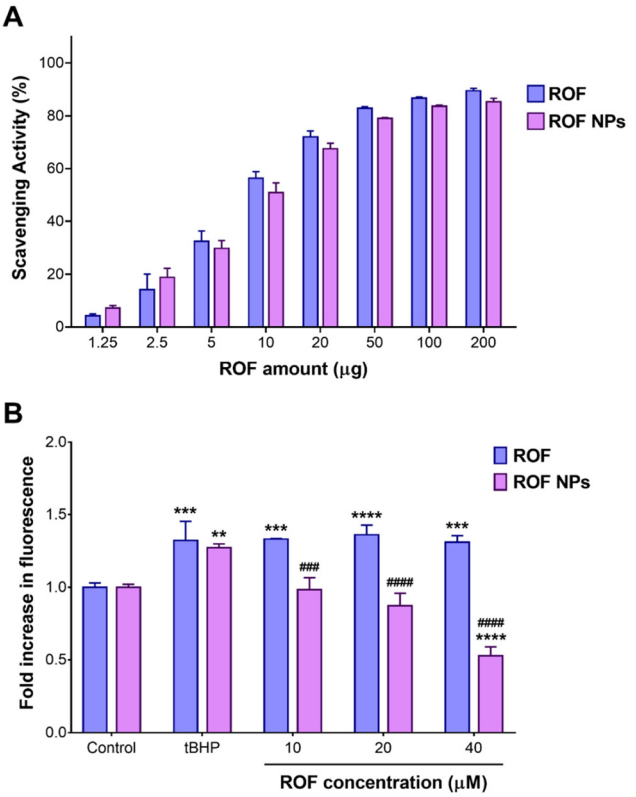

Fig. 3 (A) Antioxidant activity of ROF NPs compared to free ROF measured by the ABTS assay. Results are expressed as the average % scavenging activity ± SD (n = 3) and analyzed by 2-way ANOVA followed by Sidak's multiple comparisons test; (B) Cellular ROS scavenging activity of ROF NPs compared to free ROF in RAW 264.7 macrophages examined by a DCFDA assay. Cells (n = 3) were pretreated with various concentrations of ROF and ROF NPs for 24 h, and oxidative stress was induced by *t*BHP. Results are expressed as the average fold increase in DCF fluorescence ± SD. $^{**}p < 0.01$, $^{***}p < 0.001$, and $^{****}p < 0.0001$ compared to the control (untreated/unstimulated) cells. $^{\#\#\#}p < 0.001$ and $^{\#\#\#\#}p < 0.0001$ compared to free ROF based on 2-way ANOVA followed by Sidak's multiple comparisons test.

ROS levels in cells pretreated with ROF NPs were significantly lower than the levels obtained with equivalent concentrations of free ROF across the three tested concentrations.

Cellular uptake of NR NPs

Cellular uptake experiments were conducted using NR-labeled NPs to verify whether the observed difference in cellular ROS scavenging activity was attributed to enhanced cellular uptake of the NP formulation compared to the free drug. CLSM images of RAW 264.7 cells after 1 h of incubation with free NR and NR NPs are depicted in Fig. 4A, and the corresponding cell-associated fluorescence values are shown in Fig. 4B. Cells treated with NR NPs displayed significantly stronger intracellular red fluorescence signals compared to free NR, indicating faster uptake of the NPs compared to the free dye, which correlates with the superior intracellular antioxidant activity of the NPs compared to the free drug.

In vivo anti-inflammatory activity of ROF NPs

The anti-inflammatory activity of ROF NPs was evaluated in a formalin-induced rat paw edema model and compared to free ROF and a reference anti-inflammatory drug (DIC). Treatments were administered 1 h prior to paw edema induction and edema progression was monitored up to 24 h by measuring the fold increase in paw thickness relative to the 0 h time point. Note that the different agents were administered as a pretreatment in accordance with previous studies on ROF in animal models of inflammation.[17,18] As shown in Fig. 5A, the untreated, DIC, ROF, and ROF NPs animal groups exhibited a significant time-dependent increase in paw thickness after formalin injection compared to the control group ($p < 0.0001$), consistent with paw edema formation. The greatest fold increase in paw thickness was observed in untreated rats, which showed a steady rise from 1.4-fold (1 h post formalin injection) to 1.9-fold (24 h post formalin injection). This increase in paw thickness indicated a successful induction and persistence of paw edema over the period of the study.

Although all groups that received pretreatment with either DIC, free ROF, or ROF NPs were still associated with an increase in paw thickness compared to the control, this increase was significantly lower than the increase associated with the untreated group at all time points ($p < 0.0001$). This indicates that the pretreatment with DIC, ROF, and ROF NPs significantly inhibited edema formation and progression compared to the untreated group, confirming the anti-inflammatory activity of these drugs. Note that no significant difference was observed between DIC, free ROF, or ROF NPs across all time points, which strongly supports the potent anti-inflammatory activity of ROF alone and in the form of NPs. Morphological changes, including swelling and erythema of the rat paw in the untreated, DIC, ROF, and ROF NPs groups compared to the control group after 24 h of edema induction are presented in Fig. 5B.

The anti-inflammatory activity of ROF NPs compared to the different experimental groups was further evaluated by examining the histopathological changes in the paw tissues after 24 h of paw edema induction. The main changes are summarized in Table 6 and representative images of H & E-stained dermal layers of the paw tissues are shown in Fig. 6. Untreated animals showed significant infiltration of lymphocytes, neutrophils, and mast cells, in addition to severe vasculitis. The DIC group was associated with moderate lymphocyte infiltration, mild neutrophil infiltration, occasional appearance of mast cells, and minimal vasculitis. ROF was associated with mild lymphocyte infiltration and occasional appearance of mast cells. However, moderate neutrophil infiltration and moderate vasculitis were also observed. On the other hand, ROF NPs displayed mild lymphocyte and neutrophil infiltration with occasional appearance of mast cells and minimal vasculitis, denoting an enhancement in the anti-inflammatory activity of ROF when administered as ROF NPs.

The *in vivo* antioxidant activity of ROF NPs was also evaluated by measuring the NO levels in the inflamed paw tissues

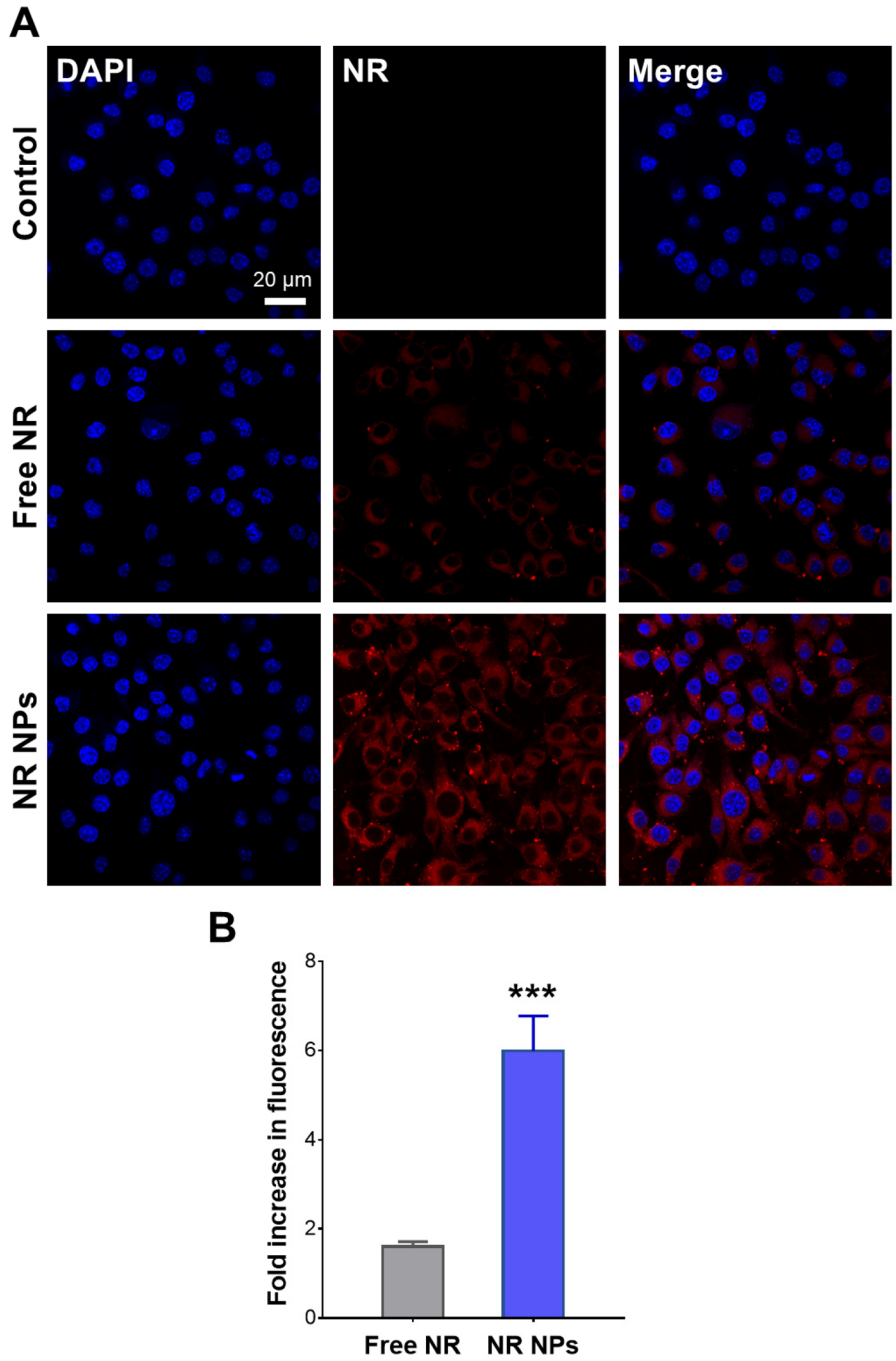

Fig. 4 Cellular uptake of NR-labeled NPs. (A) CLSM images of RAW 264.7 cells incubated with free NR or NR-labeled NPs for 1 h. Blue: cell nuclei stained with DAPI, red: NR; (B) Fold increase in fluorescence intensity of RAW 264.7 cells treated with free NR or NR-labeled NPs for 1 h relative to untreated cells. Results are expressed as the mean ± SD (n = 3). ***p < 0.001 based on unpaired t-test.

using the Griess assay for nitrite determination. As shown in Fig. 7, the untreated group displayed 2.1-fold increase in nitrite levels compared to the control group, while the groups treated with DIC, free ROF, and ROF NPs maintained normal nitrite levels, which correlates with their potent anti-inflammatory activity.

The effect of ROF NPs on slowing the progression of paw edema and the underlying inflammatory response was further supported by analyzing the gene expression of two pro-inflammatory cytokines, tnf-α and il-1β, in paw tissues extracted after 24 h of paw edema induction. TNF-α and IL-1β are important pro-inflammatory mediators as they are involved in the initiation and amplification of the inflammatory response.[52,53] RT-PCR was performed to determine the relative mRNA expression of the pro-inflammatory mediators' genes in the inflamed paw tissues. As shown in Fig. 8, the untreated group

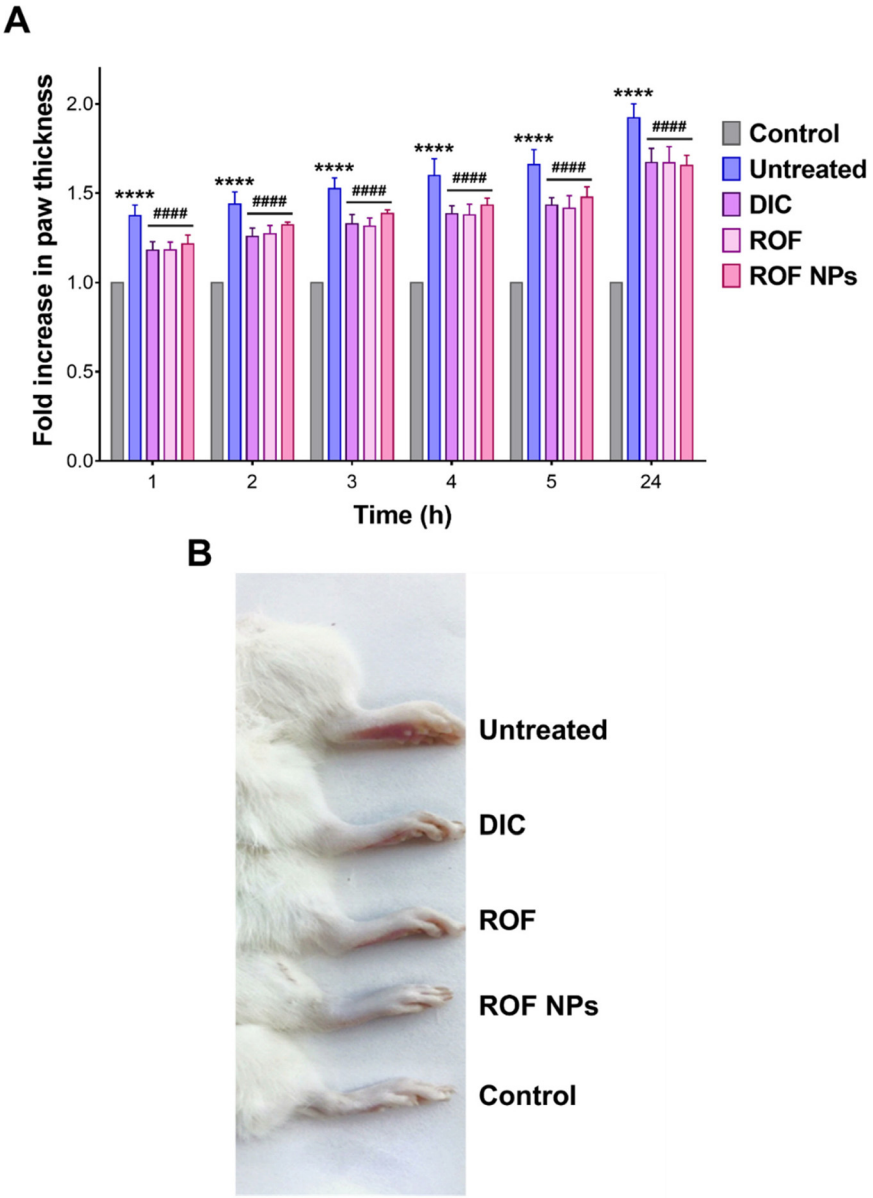

Fig. 5 *In vivo* anti-inflammatory activity of DIC, ROF, and ROF NPs. (A) Fold increase in paw thickness over a 24 h period relative to 0 h. Results are expressed as the mean fold increase in thickness ± SD (n = 5) *versus* time (h). ****$p < 0.0001$ compared to the control group and $^{\#\#\#\#}p < 0.0001$ compared to the untreated group based on 2-way ANOVA followed by Tukey's multiple comparisons test; (B) Morphological changes of the right paw of the animals after 24 h of paw edema induction.

Table 6 Histopathological changes associated with formalin-induced paw edema observed in the untreated, DIC, ROF, and ROF NPs groups compared to the control group

Group	Lymphocytes	Neutrophils	Mast cells	Vasculitis
Control	–	–	–	–
Untreated	+++	+++	+++	+++
DIC	++	+	–	–
ROF	+	++	–	++
ROF NPs	+	+	–	–

showed a significant increase ($p < 0.0001$) in both tnf-α and il-1β relative mRNA expression compared to the control, DIC, ROF, and ROF NPs groups. Moreover, groups pretreated with ROF and ROF NPs showed no significant difference in tnf-α and il-1β mRNA expression compared to the control group. Interestingly, the DIC pretreated group exhibited significantly higher ($p < 0.05$) expression of il-1β mRNA and no significant difference in tnf-α mRNA expression compared to the control group. However, the gene expression of the two cytokines was still significantly lower compared to the untreated group. The marked reduction in gene expression of the pro-inflammatory

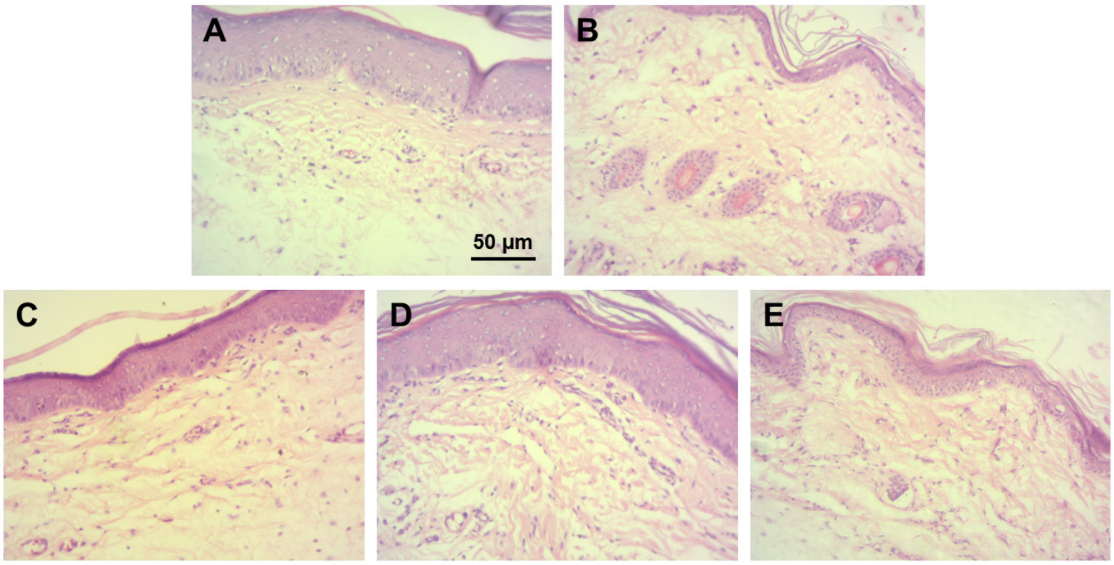

Fig. 6 Histological examination of paw tissues after 24 h of paw edema induction. Representative images from (A) control, (B) untreated, (C) DIC, (D) ROF, and (E) ROF NPs groups.

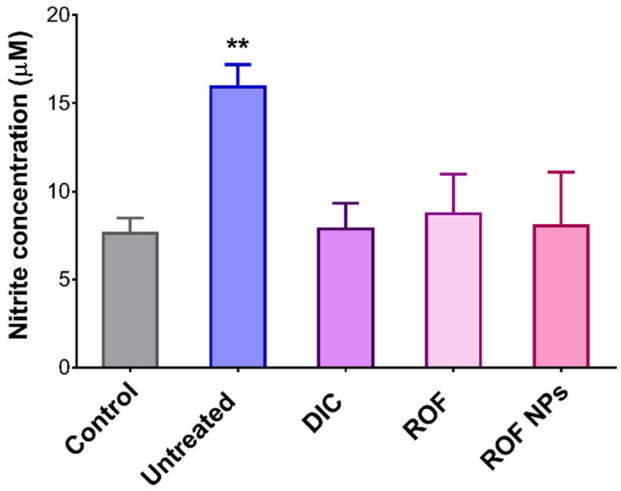

Fig. 7 Nitrite levels in paw tissues of the different animal groups after 24 h of paw edema induction. Results are expressed as the mean nitrite concentration (μM) ± SD (n = 3). **p < 0.01 compared to the control based on one-way ANOVA followed by Tukey's multiple comparisons test.

mediators confirms the anti-inflammatory activity of ROF NPs, which was comparable to free ROF and DIC.

Discussion

Poor aqueous solubility is a major challenge encountered in the development of drug candidates. Various studies have reported on polymeric NPs as drug delivery systems for different classes of drugs to enhance their solubility, efficacy and bioavailability.[54–58] In this study, we developed an NP formulation for ROF, a promising bioactive flavonoid, based on PLGA. PLGA-based polymeric NPs have been previously employed to enhance the bioavailability, biological activity, and water solubility of various natural products. For example, Derman *et al.* prepared quercetin-encapsulated PLGA NPs by the single emulsion/solvent evaporation method and the NPs showed enhanced water solubility, biocompatibility, and sustained antioxidant activity of encapsulated quercetin compared to the free drug.[59] The same technique was reported for the preparation of curcumin-loaded PLGA NPs to improve encapsulation efficiency, cytocompatibility with intestinal cells, and oral bioavailability of curcumin.[60] In another study, Feng *et al.* reported that apigenin, the aglycone of ROF, loaded into PEG–PLGA NPs had a stronger anti-inflammatory activity and longer *in vivo* circulation time than unencapsulated apigenin.[61] In another report, apigenin, was loaded in PEG–PLGA polymeric NPs to improve its solubility and bioavailability. Results demonstrated that apigenin NPs exerted an anti-inflammatory effect by inhibiting the expression and production of inflammatory cytokines and proved to be more effective in inhibiting lung fibrosis compared to free apigenin.[62]

PLGA NPs experience high rates of uptake and opsonization by the reticuloendothelial system (RES) due to their hydrophobic nature. PEGylation has been shown to be a suitable technique to enhance the colloidal stability and water solubility of polymeric NPs, prolong their systemic circulation, reduce their immunogenicity, and decrease their accumulation in the RES organs.[48,63] In this work, we used a simple and rapid technique to PEGylate ROF NPs by relying on the adhesive properties of oxidized polyphenols such as TA, avoiding the use of coupling reagents and complex purification steps. Physicochemical characterization of the optimized ROF

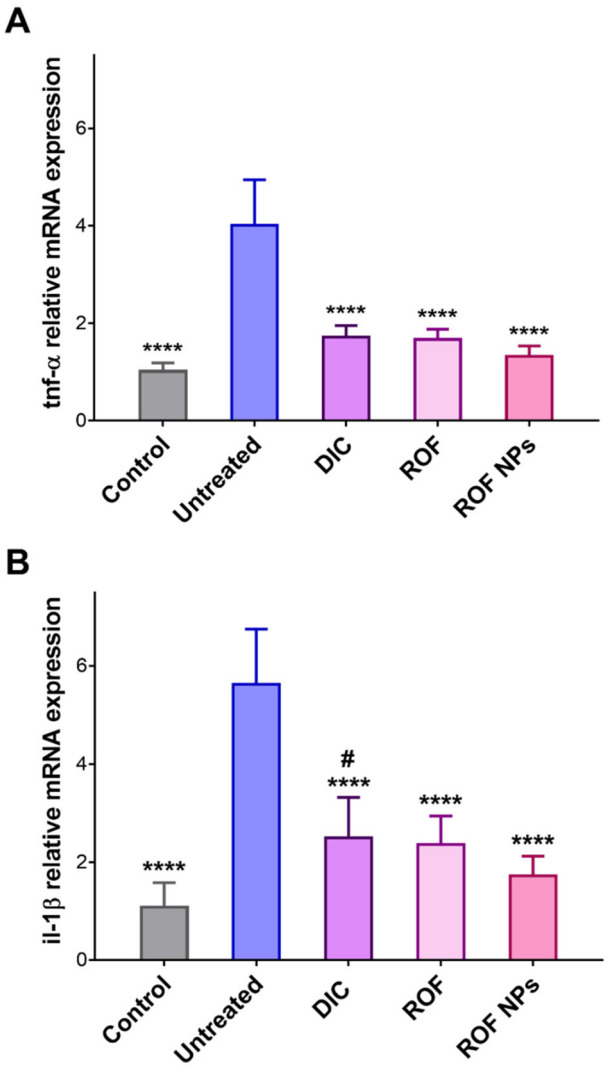

Fig. 8 *In vivo* anti-inflammatory activity of DIC, ROF, and ROF NPs. (A) tnf-α and (B) il-1β relative mRNA gene expression in paw tissues after 24 h of paw edema induction. Results are expressed as mean ± SD (n = 5) and analyzed by one-way ANOVA followed by Tukey's multiple comparisons test. ****p < 0.0001 compared to the untreated group, $^{\#}p$ < 0.05 compared to the control group.

NPs confirmed their composition and morphology. The NPs maintained excellent colloidal stability during storage and in the presence of serum, which may be attributed to the PEGylated NP surface. Similar results were obtained by our group for PEGylated polymeric nanocapsules entrapping cirsiliol, another bioactive flavonoid isolated from *T. polium*.[33] As for drug release, the relatively fast release observed during the initial hours could be explained by drug desorption from the surface of the NPs, and the sustained release pattern in the later hours may be due to slow drug diffusion and erosion of the polymeric matrix.[64] It is possible that the presence of the PEG coating increased the wettability of the hydrophobic PLGA surface, improved water permeation and drug diffusion through the polymer matrix, and consequently facilitated drug release.[65] Moreover, the ABTS antioxidant assay confirmed that loading ROF in polymeric NPs may be an appropriate approach to maintain its antioxidant activity while controlling its release. The results were consistent with those of the previous study involving cirsiliol-loaded polymeric nanocapsules.[33]

Having shown promising attributes as a delivery system for ROF, the anti-inflammatory activity of ROF NPs was evaluated in RAW 264.7 macrophages, by monitoring the levels of cellular ROS following stimulation with a hydrogen peroxide derivative, *t*BHP. ROF NPs significantly enhanced the ROS scavenging activity of free ROF and even reduced the intrinsic oxidative stress at higher concentrations. These observations may be attributed to enhanced cellular uptake of the NP formulation, similar to previous studies involving PLGA NPs as carriers for anti-inflammatory drugs.[66,67] The results were further corroborated by the cellular uptake experiments, which demonstrated faster uptake of NR-labeled NPs compared to the free dye.

Several animal models have been developed for the assessment of anti-inflammatory activities of novel drugs. Among the various animal models for inflammation, the formalin-induced paw edema model in rats has close similarity with inflammation in humans. Inflammation induced by formalin is biphasic. Bradykinin, and substance-P are involved in the early phase, whereas histamine, 5-hydroxytryptamine (5-HT), prostaglandins, and bradykinin are involved in the later phase.[68] IL-1β and TNF-α are the primary cytokines in mediating acute inflammatory reactions at the site of their production. IL-1β can stimulate T-cell proliferation, induce fever by enhancing prostaglandin E2 (PGE2) synthesis, and trigger vasodilation and increase of vascular permeability by enhancing the release of histamine from mast cells. TNF-α can also induce the acute phase response and fever, either by stimulating PGE2 synthesis or inducing the production and release of IL-1β. TNF-a and IL-1β further exert secondary inflammatory effects by stimulating IL-6 synthesis and activating the innate immune response.[52]

Recent studies have shown that the anti-inflammatory activity of ROF is mediated by affecting the production and secretion of inflammatory mediators such as TNF-α, IL-1β, and IL-6. Moreover, ROF can suppress the expression of nuclear factor kappa-B (NF-κB) signaling pathway[18] and reduce PGE2 levels[17] and the oxidative stress associated with RA.[19] Therefore, the anti-inflammatory activity of ROF NPs in the formalin-induced rat paw edema model was evaluated by monitoring the increase in paw thickness and the associated histopathological changes, and by measuring the NO and gene expression levels of tnf-α and il-1β in the inflamed paw tissues. Our results confirmed the potent anti-inflammatory activity of free ROF, which was comparable to the reference NSAID, DIC. ROF NPs exhibited an equal inhibitory effect on the progression of paw edema, tissue oxidative stress, and the gene expression levels of the pro-inflammatory mediators. However, ROF NPs performed better than the free drug in terms of mitigating the histopathological changes associated with formalin-

induced paw edema, signifying that the NPs could successfully deliver ROF to the site of inflammation.

Conclusion

In this work, the poorly soluble bioactive flavonoid ROF was isolated from *T. polium* and successfully entrapped in PLGA NPs by the emulsification/solvent evaporation method, followed by TA-mediated NP PEGylation. The effect of drug/polymer ratio and polymer concentration on NP size, polydispersity, DL, and EE was investigated to obtain the optimal NP formulation. The optimal NPs showed an average size of 204 nm with a narrow size distribution and an EE of 45%. The NPs also showed long term stability for up to 4 months and excellent stability in the presence of serum for up to 96 h. The drug release profile exhibited a biphasic pattern involving a fast initial release followed by a slower sustained release pattern for up to 96 h regardless of the pH. Antioxidant assays using ABTS demonstrated that ROF NPs maintained similar free radical scavenging activity compared to free ROF. Cellular ROS assays conducted in RAW 264.7 macrophages revealed the superiority of ROF NPs in reducing oxidative stress compared to free ROF, which correlated with the faster cellular uptake of the NPs. The *in vivo* anti-inflammatory activity of ROF NPs was investigated in a formalin-induced rat paw edema model, which confirmed the role of ROF NPs in mitigating paw edema and the histopathological signs of inflammation, most likely by ROF-mediated inhibition of oxidative stress and gene expression of pro-inflammatory cytokines such as TNF-α and IL-1β. Even though the *in vivo* anti-inflammatory activity of ROF NPs was similar to free ROF in most anti-inflammatory assays, the NP formulation offers advantages such as solubility enhancement and controlled release, which will likely prove valuable for repeated dosing by improving the pharmacokinetics and biodistribution of the free compound. Collectively, the results demonstrate the promising potential of the developed ROF NP formulation as a nanomedicine for the treatment of inflammation.

Conflicts of interest

There are no conflicts to declare.

Acknowledgements

This work received funding from Al-Zaytoonah University of Jordan (grants no. 15/28/2017-2018 and 29/11/2020-2021), and the Arab-German Young Academy of Sciences and Humanities (AGYA). AGYA draws on financial support of the German Federal Ministry of Education and Research (BMBF) grant no. 01DL20003. Isolation and spectral characterization of ROF was performed at the University of Jordan, School of Science, Department of Chemistry. The XPS data collection was performed at the Engineering and Physical Sciences Research Council (EPSRC) National Facility for XPS ("HarwellXPS"), operated by Cardiff University and University College London, under contract no. PR16195. The authors thank Dr Shaoliang Guan (School of Chemistry, Cardiff University) for assistance with XPS analysis, Dana Al-Qudah (Cell Therapy Center, University of Jordan) for assistance with CLSM imaging, and Dr Imad Hamdan (Alpha Medical Labs Pathology Consultations Center, Amman, Jordan) for assistance with histological examination.

References

1 F. R. Greten and S. I. Grivennikov, *Immunity*, 2019, **51**, 27–41.
2 M. A. Alblihed, *Mol. Biol. Rep.*, 2020, **47**, 6611–6620.
3 D. Laveti, R. Hemalatha, R. Sistla, V. Naidu, V. Talla, V. Verma, N. Kaur and R. Nagpal, *Inflammation Allergy: Drug Targets*, 2013, **12**(5), 349–361.
4 D. Furman, J. Campisi, E. Verdin, P. Carrera-Bastos, S. Targ, C. Franceschi, L. Ferrucci, D. W. Gilroy, A. Fasano, G. W. Miller, A. H. Miller, A. Mantovani, C. M. Weyand, N. Barzilai, J. J. Goronzy, T. A. Rando, R. B. Effros, A. Lucia, N. Kleinstreuer and G. M. Slavich, *Nat. Med.*, 2019, **25**, 1822–1832.
5 R. M. Haley and H. A. von Recum, *Exp. Biol. Med.*, 2019, **244**, 433–444.
6 S. Bindu, S. Mazumder and U. Bandyopadhyay, *Biochem. Pharmacol.*, 2020, **180**, 114147.
7 K. H. Maniar, I. A. Jones, R. Gopalakrishna and C. T. Vangsness Jr., *Expert Opin. Pharmacother.*, 2018, **19**, 93–102.
8 M. Salice, F. Rizzello, C. Calabrese, L. Calandrini and P. Gionchetti, *Expert Rev. Gastroenterol. Hepatol.*, 2019, **13**, 557–561.
9 T. Volmer, T. Effenberger, C. Trautner and R. Buhl, *Eur. Respir. J.*, 2018, **52**(4), 1800703.
10 N. Yahfoufi, N. Alsadi, M. Jambi and C. Matar, *Nutrients*, 2018, **10**, 1618.
11 A. Attiq, J. Jalil, K. Husain and W. Ahmad, *Front. Pharmacol.*, 2018, 976.
12 S. M. Zaidi, T. M. Al-Qirim and N. Banu, *Drugs R&D*, 2005, **6**, 157–165.
13 R. A. Khalaf, *Curr. Top. Med. Chem.*, 2016, **16**, 2549–2561.
14 M. Y. Ansari, N. Ahmad and T. M. Haqqi, *Biomed. Pharmacother.*, 2020, **129**, 110452.
15 I. Jantan, M. A. Haque, L. Arshad, H. Harikrishnan, A. W. Septama and Z.-A. Mohamed-Hussein, *J. Nutr. Biochem.*, 2021, **93**, 108634.
16 J. Refaat, S. Yehia, M. Ramadan and M. Kamel, *Int. J. Pharmacogn.*, 2015, **2**, 102–109.
17 O. Eldahshan and S. Azab, *J. Appl. Pharm. Sci.*, 2012, **2**, 74–79.
18 J. Fang, Z. Cao, X. Song, X. Zhang, B. Mai, T. Wen, J. Lin, J. Chen, Y. Chi, T. Su and F. Xiao, *Inflammation*, 2020, **43**, 2191–2201.

19 S. Peng, C. Hu, X. Liu, L. Lei, G. He, C. Xiong and W. Wu, *Braz. J. Med. Biol. Res.*, 2020, **53**(6), e9489.
20 O. Eldahshan, *Br. J. Pharm. Res.*, 2013, **3**, 46–53.
21 A. Faridi Esfanjani and S. M. Jafari, *Colloids Surf., B*, 2016, **146**, 532–543.
22 R. Conte, V. Marturano, G. Peluso, A. Calarco and P. Cerruti, *Int. J. Mol. Sci.*, 2017, **18**, 709.
23 M. Howard, B. J. Zern, A. C. Anselmo, V. V. Shuvaev, S. Mitragotri and V. Muzykantov, *ACS Nano*, 2014, **8**, 4100–4132.
24 B. Begines, T. Ortiz, M. Pérez-Aranda, G. Martínez, M. Merinero, F. Argüelles-Arias and A. Alcudia, *Nanomaterials*, 2020, **10**, 1403.
25 E. Calzoni, A. Cesaretti, A. Polchi, A. Di Michele, B. Tancini and C. Emiliani, *J. Funct. Biomater.*, 2019, **10**, 4.
26 M. Khalid and H. S. El-Sawy, *Int. J. Pharm.*, 2017, **528**, 675–691.
27 K. Park, S. Skidmore, J. Hadar, J. Garner, H. Park, A. Otte, B. K. Soh, G. Yoon, D. Yu, Y. Yun, B. K. Lee, X. Jiang and Y. Wang, *J. Controlled Release*, 2019, **304**, 125–134.
28 M. Mir, N. Ahmed and A. u. Rehman, *Colloids Surf., B*, 2017, **159**, 217–231.
29 G. Lewin, A. Maciuk, A. Moncomble and J.-P. Cornard, *J. Nat. Prod.*, 2013, **76**, 8–12.
30 K. Qabaha, T. Hijawi, A. Mahamid, H. Mansour, A. Naeem, J. Abbadi and F. Al-Rimawi, *Asian J. Chem.*, 2021, **33**, 881–884.
31 M. Khazaei, S. N. Nematollahi-Mahani, T. Mokhtari and F. Sheikhbahaei, *J. Contemp. Med. Sci.*, 2018, **4**, 1–6.
32 S. Bahramikia and R. Yazdanparast, *Phytother. Res.*, 2012, **26**, 1581–1593.
33 E. Al-Shalabi, M. Alkhaldi and S. Sunoqrot, *J. Drug Delivery Sci. Technol.*, 2020, **56**, 101544.
34 K. Kızılbey, *ACS Omega*, 2019, **4**, 555–562.
35 S. A. Abouelmagd, F. Meng, B.-K. Kim, H. Hyun and Y. Yeo, *ACS Biomater. Sci. Eng.*, 2016, **2**, 2294–2303.
36 L. Pang, Y. Pei, G. Uzunalli, H. Hyun, L. T. Lyle and Y. Yeo, *Pharm. Res.*, 2019, **36**, 65.
37 J. Shen and D. J. Burgess, *Drug Delivery Transl. Res.*, 2013, **3**, 409–415.
38 S. Sunoqrot, E. Al-Shalabi, A. G. Al-Bakri, H. Zalloum, B. Abu-Irmaileh, L. H. Ibrahim and H. Zeno, *ACS Omega*, 2021, **6**, 2767–2776.
39 L. Wang, M. L. Xu, J. H. Hu, S. K. Rasmussen and M.-H. Wang, *Food Chem. Toxicol.*, 2011, **49**, 149–154.
40 G. Li, J. Zhou, M. Sun, J. Cen and J. Xu, *J. Funct. Foods*, 2020, **74**, 104196.
41 A. Soyocak, H. Kurt, D. T. Cosan, F. Saydam, I. Calis, U. Kolac, Z. O. Koroglu, I. Degirmenci, F. S. Mutlu and H. Gunes, *Hum. Exp. Toxicol.*, 2019, **38**, 1296–1301.
42 C.-W. Chang, W.-T. Chang, J.-C. Liao, Y.-J. Chiu, M.-T. Hsieh, W.-H. Peng and Y.-C. Lin, *J. Evidence-Based Complementary Altern. Med.*, 2012, 135379.
43 A. Peinnequin, C. Mouret, O. Birot, A. Alonso, J. Mathieu, D. Clarençon, D. Agay, Y. Chancerelle and E. Multon, *BMC Immunol.*, 2004, **5**, 3.
44 K. J. Livak and T. D. Schmittgen, *Methods*, 2001, **25**, 402–408.
45 A. K. Yadav, D. Yadav, K. Shanker, R. K. Verma, A. K. Saxena and M. M. Gupta, *Chromatographia*, 2009, **69**, 653–658.
46 F. Masood, *Mater. Sci. Eng., C*, 2016, **60**, 569–578.
47 N. Sharma, P. Madan and S. Lin, *Asian J. Pharm. Sci.*, 2016, **11**, 404–416.
48 N. Bertrand, P. Grenier, M. Mahmoudi, E. M. Lima, E. A. Appel, F. Dormont, J.-M. Lim, R. Karnik, R. Langer and O. C. Farokhzad, *Nat. Commun.*, 2017, **8**, 777.
49 T. S. Sileika, D. G. Barrett, R. Zhang, K. H. A. Lau and P. B. Messersmith, *Angew. Chem., Int. Ed.*, 2013, **52**, 10766–10770.
50 J. Yoo and Y.-Y. Won, *ACS Biomater. Sci. Eng.*, 2020, **6**, 6053–6062.
51 H. Zhang and R. Tsao, *Curr. Opin. Food Sci.*, 2016, **8**, 33–42.
52 C. A. Feghali and T. M. Wright, *Front. Biosci.*, 1997, **2**, d12–d26.
53 A. A. M. Abd-Allah, N. El-Deen, W. A. M. Mohamed and F. M. Naguib, *Iran. J. Basic Med. Sci.*, 2018, **21**, 97–107.
54 D. Beconcini, F. Felice, Y. Zambito, A. Fabiano, A. M. Piras, M. H. Macedo, B. Sarmento and R. Di Stefano, *Pharmaceutics*, 2019, **11**, 500.
55 G. M. Pontes-Quero, L. Benito-Garzón, J. Pérez Cano, M. R. Aguilar and B. Vázquez-Lasa, *Pharmaceutics*, 2021, **13**, 290.
56 S. Sunoqrot and L. Abujamous, *J. Drug Delivery Sci. Technol.*, 2019, **52**, 670–676.
57 S. Sunoqrot, M. Alfaraj, A. a. M. Hammad, V. Kasabri, D. Shalabi, A. A. Deeb, L. Hasan Ibrahim, K. Shnewer and I. Yousef, *Pharmaceutics*, 2020, **12**, 811.
58 B. Yang, Y. Dong, F. Wang and Y. Zhang, *Molecules*, 2020, **25**, 4613.
59 S. Derman, D. Uzunoglu, T. Acar, T. Ozbek Arasoglu, S. Ucak, V. Ozalp and B. Mansuroglu, *Iran. J. Pharm. Res.*, 2020, **19**, 424–435.
60 A. Umerska, C. Gaucher, F. Oyarzun-Ampuero, I. Fries-Raeth, F. Colin, M. G. Villamizar-Sarmiento, P. Maincent and A. Sapin-Minet, *Antioxidants*, 2018, **7**, 46.
61 W.-m. Feng, H.-h. Guo, T. Xue, X. Wang, C.-w. Tang, B. Ying, H. Gong and G. Cui, *RSC Adv.*, 2015, **5**, 83628–83635.
62 J. Zhang, L. Chao, X. Liu, Y. Shi, C. Zhang, L. Kong and R. Li, *Exp. Lung Res.*, 2017, **43**, 359–369.
63 Z. Zhao, A. Ukidve, V. Krishnan and S. Mitragotri, *Adv. Drug Delivery Rev.*, 2019, **143**, 3–21.
64 N. Kamaly, B. Yameen, J. Wu and O. C. Farokhzad, *Chem. Rev.*, 2016, **116**, 2602–2663.
65 N. M. Khalil, T. C. F. d. Nascimento, D. M. Casa, L. F. Dalmolin, A. C. d. Mattos, I. Hoss, M. A. Romano and R. M. Mainardes, *Colloids Surf., B*, 2013, **101**, 353–360.
66 F. Y. Siu, S. Ye, H. Lin and S. Li, *Int. J. Nanomed.*, 2018, **13**, 4133–4144.
67 J. Pinto, M. Ahmad and B. R. Guru, *J. Biomater. Sci., Polym. Ed.*, 2019, **30**, 1188–1211.
68 K. R. Patil, U. B. Mahajan, B. S. Unger, S. N. Goyal, S. Belemkar, S. J. Surana, S. Ojha and C. R. Patil, *Int. J. Mol. Sci.*, 2019, **20**, 4367.